Inverse problem approaches for stationary Fourier transform spectrometers

Frédéric Gillard,[1,*] Sidonie Lefebvre,[1] Yann Ferrec,[1] Laurent Mugnier,[1] Sylvain Rommeluère,[1] Céline Benoit,[1] Nicolas Guérineau,[1] and Jean Taboury[2]

[1]*ONERA—The French Aerospace Lab, F-91761, Palaiseau, France*

[2]*Laboratoire Charles Fabry, Institut d'Optique, Université Paris-Sud, CNRS, 2 avenue Augustin Fresnel, F-91127 Palaiseau cedex, France*

**Corresponding author: frederic.gillard@onera.fr*

Received May 10, 2011; revised May 26, 2011; accepted May 31, 2011; posted May 31, 2011 (Doc. ID 147161); published June 21, 2011

A design of a miniaturized stationary Fourier transform IR spectrometer has been developed that produces a two-dimensional interferogram. The latter is disturbed by effects like parasitic interferences or disparities in the cutoff wavelength of the pixels. Thus, a simple Fourier transform cannot be used to estimate the spectrum of the scene. However, as these defects are deterministic, they can be measured and taken into account by inversion methods. A regularization term can also be added. The first experimental results prove the efficiency of this processing methodology. © 2011 Optical Society of America

OCIS codes: 040.3060, 300.6190, 100.3190.

We have recently proposed a new design of Fourier transform IR (FTIR) spectrometer [1] that operates without the need for a scanning mechanism. The approach consists of designing and building an IR focal plane array (FPA) containing a simple modification that turns it into a stationary FTIR spectrometer. Thus, the spectrometer can be made quite compact, and, ultimately, the entire IR system could be integrated in a Dewar, leading to a handheld and cryogenic FTIR spectrometer [2]. Such an instrument is dedicated to specific applications requiring high radiometric performances, such as the spectral analysis of natural samples at room temperature or the time-resolved measurements of spectra emitted by chemical agents. The innovative process of the FPA leaves a wedge-shaped and uncoated substrate on the active layer of the array. When this device is illuminated by an IR source, we obtain a two-dimensional (2D) interferogram, which is the result of interferences inside the wedge. Figure 1 illustrates examples of images produced by an FTIR FPA under quasi-monochromatic light. These images have been obtained thanks to a spectral characterization [3] that leads to a hyperspectral cartography of our spectrometer.

Usually, a Fourier transform (FT) is used to process the 2D interferogram in order to estimate the spectrum of the source. However, in our case, three principal reasons prevent us from using a classic FT. First of all, because of the nonplanarity of the wedge, the interferogram is not regularly sampled on the detector, leading to curved optical fringes, as illustrated in Fig. 1(a). A solution to this problem is to compute the FT over a one-dimensional (1D) interferogram extracted from the image using a precise 2D cartography of the optical path difference in front of each pixel of the array [1]. Second, the interferogram is not the result of two wave interferences (as in the Michelson interferometer case). In particular, at high wavelengths (near the cutoff wavelength of the absorbing layer, see Fig. 1(b)), a third wave interferes that encodes thickness inhomogeneities of the absorbing (HgCdTe) layer [3]. It leads to a wavelength-dependent distortion of the optical fringes contrast. In this case, the technique of rearranging the interferogram can no longer be applied. Third, spatial inhomogeneities of pixel responses generate additional noise called fixed pattern noise (FPN) that spreads out the peaks of the FT. As for imagers, strategies of correction can be implemented. But these strategies (two-point correction for example) are valuable for a given spectral bandwidth. In our case, wavelength-dependent FPN appears due to inhomogeneities of the cutoff wavelengths of the pixels. For all these reasons, FT-based processing cannot be applied to our device. In this Letter, we introduce a more sophisticated processing methodology.

The FTIR FPA delivers an m_x elements $\times$ m_y elements interferogram. The optical path difference evolves on the detector from the null path difference on the edge of the wedge-shaped substrate to $\delta_{\max}$ on the opposite side. Each pixel of the detector has its own optical path difference, but we notice a lot of redundancies because of the near-planarity of the wedge. The interferogram's data are concatenated into a 1D vector denoted Y of size m(equal to $m_x \times m_y$). The spectrum is a vector of data denoted X of size n, where n is the number of wavenumbers. Thanks to the linearity of the detection process, we can write the direct problem equation as

$$Y = MX + \text{noise}. \tag{1}$$

The transition matrix M of size $m \times n$ must be filled with the responses of the m pixels of the detector at the n

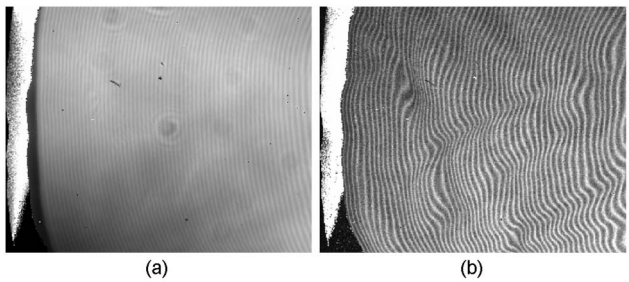

(a) (b)

Fig. 1. (a) Hyperspectral cartography at 4 μm; (b) hyperspectral cartography at 5.2 μm.

wavenumbers, i.e., with the hyperspectral cartographies of each wavelength. In order to estimate the spectrum, we need to invert Eq. (1). Because M is not square, we can not use a simple inversion. An estimation of the pseudoinverse $M^{\dagger}$ can be obtained by singular value decomposition (SVD) of M, and $\hat{X} = (M^T M)^{-1} M^T Y$ is then the classic least squares solution $\arg\min(\|Y - MX\|_2^2)$. In order to make the most of *a priori* information and spectra, one can apply instead regularized inversion methods. The estimation of X is then the result of the minimization of the data-fidelity term plus a regularization term $R(X)$. We have

$$\hat{X} = \arg\min(\|Y - MX\|_2^2 + \alpha R(X)). \tag{2}$$

Many forms of regularization terms exist in the literature. The most popular ones in the context of spectral estimation have been tested on our experimental data.

In this Letter, we present three inversion methods that led to promising results. The first method (method (a)) is truncated SVD (TSVD). TSVD is a standard approach that does not introduce *a priori* knowledge of the searched spectrum (positivity, smoothness). As M is ill conditioned, many of the singular values of the SVD decomposition, while not zero, can become quite small, causing the data inversion to blow up if there is any noise. This explains why we resort to TSVD by neglecting components of the solution corresponding to the smallest singular values. The truncation order adjustment is the main difficulty of this approach. The next two methods are regularized approaches [4] that include *a priori* knowledge of the spectrum (method (b)) or of the coefficients of the spectrum decomposition on a wavelet basis (method (c)). The second method assumes a regularization operator R that takes the form of a finite difference operator, leading to smooth solutions for $\hat{X}$: we assume that the spectrum does not vary very fast. The third method takes advantage of compressed sensing results [5]: a small number of random projections of a sparse signal can contain its salient information. R then takes the form of a penalization on the L1 norm of the coefficients of X decomposition on a wavelet basis, where the L1 norm is defined as the sum of the modulus of X coordinates,. The L1 term compels small coefficients to become exactly zero, thus promoting sparse solutions. For the two last methods, the α is currently tuned by the user in order to reach an appropriate trade-off between *a priori* information and data fidelity. In the same way, for the TSVD processing, the truncation order must be optimized.

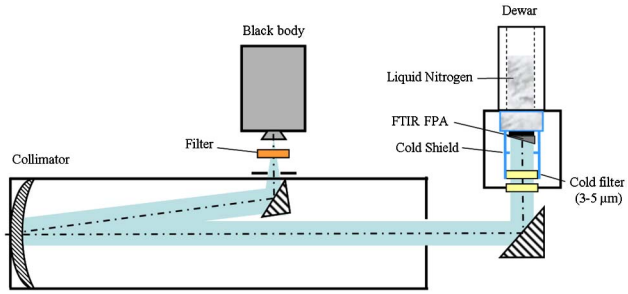

Fig. 2. (Color online) Experimental setup for the measurement of spectral filters.

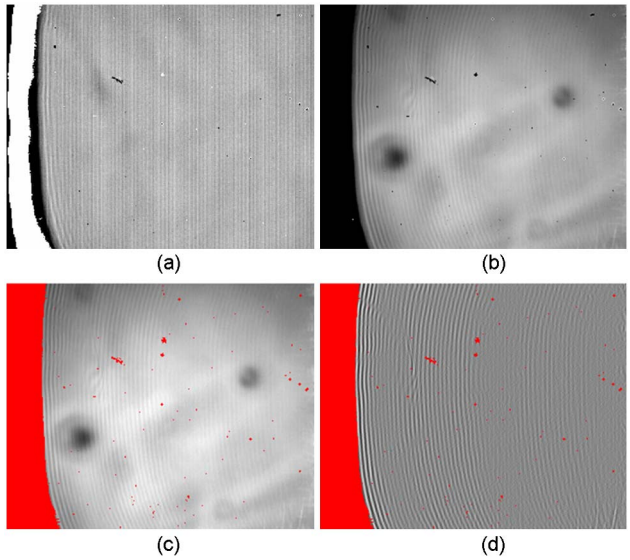

Fig. 3. (Color online) Preprocessing of an interferogram [in (c) and (d), the dead pixels are indicated in red].

To demonstrate the validity of our processing method, we have carried out the following experiment (Fig. 2): we illuminate our FTIR FPA with a black body at a temperature of 1000 K and a collimator. A reference filter is placed after the black body. The source spectrum encoded by the interferogram is the product of the black body spectrum, the atmospheric transmission spectrum, and the filter spectral transmission. In order to estimate the spectrum, we need to fill in M and to inverse it. For this, we use the experimental data produced by our hyperspectral study. The result of the spectral characterization is a three-dimensional $[m_x, m_y, z]$ data set made of z images of size $[m_x, m_y]$, with z the number of wavenumbers and $[m_x, m_y]$ the size of the FPA. Each image is the monochromatic response of our FPA, as illustrated in Figs. 1(a) and 1(b). We are able to fill M with a spectral resolution of $1\,\mathrm{cm}^{-1}$. The acquired 2D interferogram, as well as the hyperspectral cartography, are preprocessed before applying inversion methods. Indeed, we want to fill M with the response of the sensor in the same

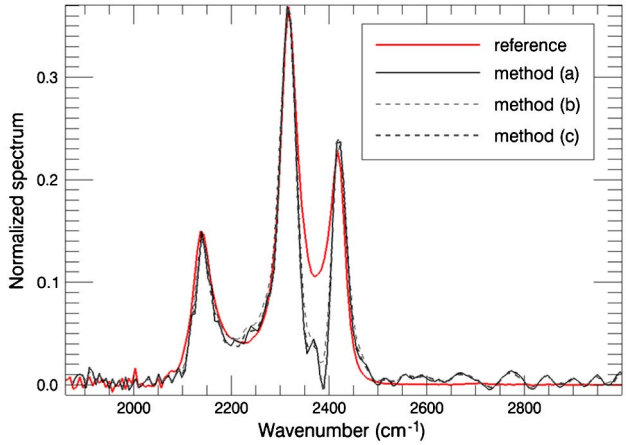

Fig. 4. (Color online) Filter A transmission estimations by the three methods: method (a), TSVD; method (b), regularized inversion; method (c), regularized inversion on a wavelet basis. Around $2400\,\mathrm{cm}^{-1}$, CO_2 absorption is eliminated in the reference spectrum.

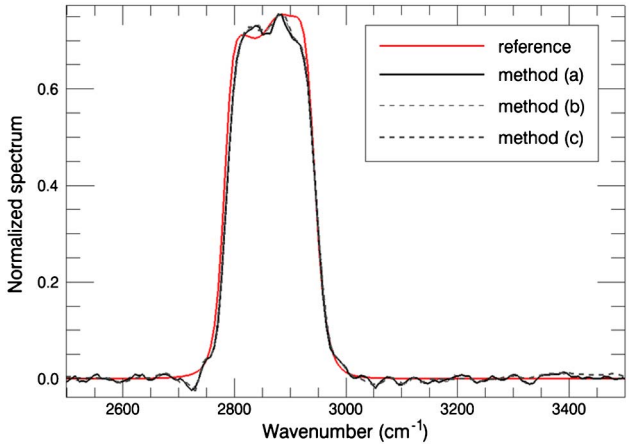

Fig. 5. (Color online) Filter B transmission estimations by the three methods: method (a), TSVD; method (b), regularized inversion; method (c), regularized inversion on a wavelet basis.

conditions as the experimental ones. First, a raw image [Fig. 3(a)] is tainted by the electric offset. We measure this offset by illuminating the instrument with a cold (77 K) background and we subtract it on each image (on the experimental interferogram and on each image of the hyperspectral cartography), leading to Fig. 3(b). Second, we detect dead pixels. All the detected dead pixels are eliminated both from the interferogram and from the hyperspectral cartography. Dead pixels are depicted in red in Fig. 3(c). Third, we process the images in order to obtain interferograms that have a constant average. A low-pass filter is applied to each image, giving the low frequency profile of the image. This profile is divided on the image [Fig. 3(d)] to correct the variations of the lighting conditions. We fill the M matrix with the processed hyperspectral cartography and the Y vector with the processed interferogram. We can now proceed to the inversion step.

Figures 4 and 5 show estimations of two filters' (A and B) transmissions with the three methods. A reference transmission has been measured for both filters with a commercial FTIR. For each method, we present the estimation obtained with the optimal truncation order or the optimal α value. The match between the reference transmission and the transmission curves estimated with the three methods is very good despite repeatable artifacts at wavenumbers beyond the cutoff of the filter and random noise appearing at low wavenumbers. These differences come from the calibration and preprocessing steps that are not yet optimal. It should be mentioned that we are currently working on them to obtain more reliable spectra. The regularized methods seem to be a little more accurate than the TSVD, leading to smoother results. Note that the gap between the estimated A spectra and the reference in the 2350–2420 cm^{-1} range is due to the absorption of the atmospheric CO_2, which is experimentally eliminated in the reference spectrum measurement.

In conclusion, inversion methods applied to Fourier-transform spectrometry are a promising way to process stationary interferograms. A key element is the characterization of the instrument. Different inversion methods have been tested on experimental data. It seems that the three methods presented in this Letter give an effective estimation of a filter transmission. Note that our processing method can be used with other FT spectrometers [6,7].

References

1. S. Rommeluère, N. Guérineau, R. Haidar, J. Deschamps, E. De Borniol, A. Million, J.-P. Chamonal, and G. Destefanis, Opt. Lett. **33**, 1062 (2008).
2. F. Gillard, N. Guérineau, S. Rommeluère, J. Taboury, and P. Chavel, Proc. SPIE **7716**, 77162E (2010).
3. S. Rommeluère, R. Haïdar, N. Guérineau, J. Deschamps, E. De Borniol, A. Million, J. P. Chamonal, and G. Destefanis, Appl. Opt. **46**, 1379 (2007).
4. J. Idier, *Bayesian Approach to Inverse Problems* (Wiley ISTE, 2008).
5. M. A. T. Figueiredo, R. D. Nowak, and S. J. Wright, IEEE J. Sel. Top. Signal Process. **1**, 586 (2007).
6. E. le Coarer, S. Blaize, P. Benech, I. Stefanon, A. Morand, G. Lérondel, G. Leblond, P. Kern, J. M. Fedeli, and P. Royer, Nat. Photon. **1**, 473 (2007).
7. P. G. Lucey, K. A. Horton, and T. Williams, Appl. Opt. **47**, F107 (2008).